

# Autocatalytic avalanches of unit inelastic shearing events are the mechanism of plastic deformation in amorphous silicon

Michael J. Demkowicz<sup>1,2,\*</sup> and Ali S. Argon<sup>1</sup>

<sup>1</sup>*Department of Mechanical Engineering, Massachusetts Institute of Technology, Cambridge, Massachusetts 02139, USA*

<sup>2</sup>*MST-8: Structure-Property Relations, Los Alamos National Laboratory, Los Alamos, New Mexico 87545, USA*

(Received 29 April 2005; revised manuscript received 29 September 2005; published 20 December 2005)

Discrete stress relaxations were found to be the source of low-temperature plastic flow in amorphous silicon (a-Si) as modeled by atomistic simulation using the Stillinger-Weber potential. These relaxations are triggered when a local yielding criterion is satisfied in a small cluster of atoms. The atomic rearrangements accompanying discrete stress relaxations are describable as autocatalytic avalanches of unit shearing events. Every such unit event centers on a clearly identifiable change in bond length between the two split peaks of the second nearest-neighbor shell in the radial distribution function of bulk a-Si in steady-state flow.

DOI: [10.1103/PhysRevB.72.245206](https://doi.org/10.1103/PhysRevB.72.245206)

PACS number(s): 61.43.Dq, 61.43.Fs, 62.20.Fe, 81.05.Gc

## I. INTRODUCTION

In a previous atomistic simulation study of plastic flow in amorphous silicon (a-Si),<sup>1,2</sup> it was demonstrated that individual atomic environments could be unambiguously classified as either solidlike or liquidlike. The mass fraction  $\phi$  of liquidlike atomic environments was found to act as a plasticity carrier, i.e., a-Si systems with larger values of  $\phi$  are more amenable to plastic flow. Thus,  $\phi$  plays a role in a-Si similar to that of free volume in metallic glasses,<sup>3</sup> both with respect to plastic flow as well as aging.<sup>4,5</sup> In addition to its connection to average mechanical response, however, the liquidlike-solidlike distinction indicates the possibility of finding repeatable inelastic atomic-level structure changes associated with the transformation of liquidlike atomic environments to solidlike ones and vice versa. In other words, it suggests the existence of a specific mechanism of plastic flow in a-Si.

It might not be, at first, intuitively clear that amorphous solids can exhibit any repeatable mechanism of plasticity. Nevertheless, early investigations of inelastic transformation in model two-dimensional metallic glasses using the bubble-raft method<sup>6</sup> as well as atomistic simulations with pair potentials<sup>3</sup> found that plasticity in these materials initiates at sites of high free volume and proceeds in a series of localized structure transformations involving clusters of about 10 atoms. This finding invalidated the Eyring hypothesis<sup>7</sup> for flow in glassy solids. It also proved that no form of “generalized dislocations” mediate plasticity in such materials.<sup>8</sup> More importantly, however, the studies of plasticity in model metallic glasses suggested the possibility of the existence of distinct mechanisms of inelastic structure transformation in amorphous materials.

Building upon this realization, Bulatov and Argon<sup>4</sup> constructed a simplified model of metallic glasses that presupposed a single plastic deformation mechanism that could be activated by both thermal motion and mechanical stresses. This assumption was meant to combine the observations that plastic deformation in glassy metals is local and occurs preferentially at certain sites. Through a series of simulations, Bulatov showed that if interactions between inelastically transforming regions and the surrounding elastically deform-

ing matrix material are taken into account, a single deformation mechanism is able to reproduce all of the high- and low-temperature behaviors observed in metallic glasses. The model of Bulatov and Argon uses several material parameters to characterize the form of thermal and mechanical activation behavior of unit plastic events, but makes no reference to their origin. In particular, these parameters could be extracted from atomistic simulations of plasticity in materials governed by any interaction law, provided that unit plastic deformation events indeed exist in these materials. The general conclusions of the Bulatov-Argon model would therefore be expected to apply to disordered covalently bonded materials as much as to metallic glasses.

Investigations of a-Si in the context of phenomena other than plastic flow under external loading have given rise to hopes of isolating individual mechanisms of structure transformation responsible for those phenomena. For example, Bernstein *et al.* conducted atomistic simulations to search for mechanisms of solid-phase epitaxial growth (SPEG) of crystalline silicon (c-Si) from a-Si.<sup>9</sup> Meanwhile, Valiquette and Mousseau characterized thermal excitation-induced structure transitions in relaxed a-Si configurations.<sup>10</sup> The study presented here is an investigation of the atomic mechanisms of plasticity in a-Si.

## II. METHODS

The research presented here made use of the same model for Si as the one adopted by the authors in the study that motivated the current work.<sup>1,2</sup> Namely, the Stillinger-Weber (SW) potential<sup>11</sup> was chosen from among other commonly used empirical models<sup>12–14</sup> because of its simple design, the extent to which its behavior has been previously explored, and its lack of stark, unphysical deviations from the behavior of real Si.<sup>15–19</sup> All simulations were carried out under periodic boundary conditions on configurations consisting of 4096 atoms, i.e.,  $8 \times 8 \times 8$  cubic unit cells of the diamond cubic crystalline configuration.

Amorphous Si systems of varying densities were created by melting crystalline Si (c-Si) and quenching it at different rates, as previously described.<sup>1,2</sup> Four representative a-Si

systems of differing densities were then deformed by externally applying small increments of volume conserving plane strain<sup>20</sup> to the simulation cell and equilibrating the system after the application of each strain increment. These externally applied strain increments consisted of an extension increment  $d\epsilon_x$  in the  $x$  direction and the same amount of contraction increment  $d\epsilon_y$  in the  $y$  direction (since the constant volume requirement in this loading mode requires  $d\epsilon_y = -d\epsilon_x/(1+d\epsilon_x)$ , the amount of contraction increment applied in the  $y$  direction was actually very slightly less than extension in the  $x$  direction). The system length in the  $z$  direction was held fixed. In the work that motivated this study,<sup>1,2</sup> relaxation of externally strained structures was accomplished using molecular dynamics (MD) simulation at a constant temperature of  $T=300$  K. Because the thermal motion of atoms in MD simulations obscures the intimate details of individual atomic-level structure transformations, however, the mechanisms of plasticity in a-Si are most conveniently studied using the effectively zero-temperature relaxation technique of potential-energy minimization (PEM).<sup>21</sup>

PEM relaxations were performed using the Polak-Ribiere conjugate gradient method<sup>22</sup> with restarts.<sup>23</sup> Conjugate gradient minimization was terminated when the total force on each atom decreased below  $10^{-8}$  times the characteristic force of the SW potential ( $1.66 \times 10^{-9}$  N). Trust region Newton-Raphson minimization steps<sup>23</sup> were subsequently applied until the total force on each atom decreased below  $10^{-14}$  times the characteristic force of the SW potential, yielding very finely equilibrated atomic structures. Whenever the energy minimum of the atomic system was too ill-conditioned for either the conjugate gradient or Newton-Raphson techniques to work—as is sometimes the case near the mechanical threshold of plastic relaxations (Sec. VII)—a line minimization was carried out using the robust algorithm due to Brent<sup>24</sup> (available online at Netlib<sup>25</sup>) along the direction of the lowest stiffness nontranslational eigenmode of the system Hessian matrix. To accurately resolve all mechanical instabilities arising during a mechanical deformation simulation using PEM relaxation, volume-conserving plane-strain increments with  $d\epsilon_x = 3.2 \times 10^{-5}$  were applied.

The PEM methods described above as well as some of the structural analysis methods to be described later make use of the matrix of second derivatives of the system potential with respect to atomic positions (i.e., the stiffness or Hessian matrix). This matrix can be calculated directly from the form of the SW potential and stored in sparse vector form.<sup>26</sup> Solutions of linear systems involving the Hessian matrix were found using the SYMMLQ iterative scheme<sup>27</sup> (available online at Netlib<sup>25</sup>). Selected eigenvalues and eigenvectors of the Hessian matrix were determined as needed using the ARPACK implementation of the Implicitly Restarted Arnoldi Method (IRAM),<sup>28</sup> available online at Netlib.<sup>25</sup>

The method of finding the mass fraction  $\phi$  of liquidlike atomic environments for any a-Si system was described in Refs. 1 and 2. The full system stress tensor  $\boldsymbol{\tau}$  was calculated directly from the form of the SW potential as described in Ref. 2. It is useful to decompose the components  $\tau_{ab}$  of the system stress into  $i=1 \dots, N$  contributions  $(\tau_{ab})_i$  associated with atomic sites subject to the constraint

$$\tau_{ab} = \frac{1}{N} \sum_{i=1}^N (\tau_{ab})_i. \quad (1)$$

The quantities  $(\tau_{ab})_i$  are called the atomic-site stress tensor elements, following Maeda and Takeuchi.<sup>29</sup> Because a-Si is an isotropic material, the results of mechanical deformation simulations are conveniently stated in terms of the pressure  $p$  and deviatoric  $\bar{\boldsymbol{\sigma}}$  components of the stress tensor  $\boldsymbol{\tau}$ .<sup>20</sup> These components are defined as

$$p(\boldsymbol{\tau}) = -\frac{1}{3} \text{tr}(\boldsymbol{\tau}) \quad (2a)$$

$$\bar{\boldsymbol{\sigma}}(\boldsymbol{\tau}) = \left| \boldsymbol{\tau} - \frac{1}{3} \text{tr}(\boldsymbol{\tau}) \mathbf{I} \right|, \quad (2b)$$

where  $\text{tr}$  stands for the tensor trace and  $\mathbf{I}$  for the identity tensor. Deviatoric stress accounts for all shearing stresses and excludes all dilatational stress components. Both pressure and deviatoric stress can be computed for the system-wide stress tensor as well as for all atomic-site stress tensors. Although system-wide  $p$  and  $\tau_{ab}$  are averages over the volume of corresponding atomic-site quantities, however, the system-wide deviatoric stress is not the average over the volume of atomic-site deviatoric stresses. Rather, it is the deviatoric component of the volume average atomic-site stress tensors. Deviatoric strain  $\bar{\boldsymbol{\epsilon}}$  is computed from the strain tensor  $\boldsymbol{\epsilon}$  analogously to deviatoric stress.

Previous studies<sup>9,10</sup> of mechanisms of structure transformations in a-Si for phenomena other than plastic flow reveal the importance of developing appropriate methods of “pattern recognition” to extract recurring features from large sets of events. Certain such methods tailored to the needs of studies of stress-induced inelastic deformation have made their appearance in work on dry foams<sup>30</sup> and silica glass.<sup>31</sup> Several pattern recognition approaches have been developed specifically for the work presented here and will be described as they arise in the following sections.

### III. COMPARISON OF PLASTIC DEFORMATION BY MD AND PEM

It was claimed in Sec. II that the method of PEM is preferable to finite-temperature MD simulation as a means of studying the mechanisms of inelastic relaxation in a-Si. The constant volume deformation behavior found previously by MD simulation<sup>1,2</sup> was therefore compared to effectively zero-temperature constant volume deformation behavior as simulated by PEM. The four series of configurations generated by constant volume deformation using MD were used as points of reference for the PEM simulations carried out afterward: every configuration in each series was brought to its closest equilibrium configuration by setting all of its atomic velocities to zero (effectively removing all thermal motion) and bringing the system potential energy to its nearest local minimum by relaxing it with respect to the atomic positions. A particular configuration was then chosen from each of the four series as a starting point for deformation using PEM simulation. In order to decrease the computation costs in the relatively uninteresting regime of “elasticlike” deformation (amorphous solids have no true elastic limit, but show iso-

lated inelastic relaxations separated by regions of reversible deformation behavior even at low stress levels<sup>3,32</sup>), these initial structures were chosen from among highly strained configurations in each of the four series generated by MD simulation.

Figure 1 compares the mechanical behavior of a-Si when deformed plastically at constant volume by MD at  $T = 300$  K and by PEM. The changes in pressure [Fig. 1(b)] as well as the variations of liquidlike mass fraction  $\phi$ <sup>1,2</sup> [Fig. 1(c)] exhibit closely similar trends for the two simulation methods, suggesting that the same mechanisms are responsible for plasticity in both cases. Finite temperature deformation using MD, however, exhibits a markedly decreased level of flow stress [Fig. 1(a)] when compared to the PEM case.<sup>33,34</sup> This effect has been attributed before to temperature dependence of the elastic moduli and thermal activation of the atomic rearrangements that lead to plasticity,<sup>33</sup> but has not been found to alter the mechanism of stress relaxation itself.

#### IV. DISCRETE STRESS RELAXATIONS AS THE SOURCE OF PLASTIC FLOW IN a-Si

Closer inspection of a section of a typical stress-strain curve obtained using PEM (presented in Fig. 2) reveals that it is composed of regions of smooth, reversible variation of stress separated by sudden isolated, discrete, and irreversible stress relaxations, each occurring at a well-defined mechanical threshold stress [Figs. 2(a) and 2(b)]. As in the case of glassy polymers<sup>32</sup> and metallic glasses,<sup>35,36</sup> such irreversible stress relaxations are the source of inelastic behavior in a-Si. The ensemble average of large numbers of these events is responsible for the apparently smooth overall plastic deformation behavior of large samples of a given material. Figure 2(c) shows that the largest changes in liquidlike mass fraction  $\phi$  coincide with the largest stress relaxations. Nevertheless, some fluctuations in  $\phi$  do occur in regions of reversible stress variation, indicating that although changes in the nature of atomic environments are induced primarily by inelastic stress relaxations, they can also result from some elastic flexing of bond angles.

A total of 4201 discrete stress relaxations were observed in the course of the four series of PEM deformation simulations summarized in Fig. 1. This set of stress relaxations forms the basis for the analyses presented in this and subsequent sections. These analyses always yielded the same results regardless of whether the stress relaxations in the four deformation runs were analyzed separately or together. The reason for this lack of differentiation among the four simulation runs will be addressed in Sec. VII.

The intensity of each relaxation can be described by finding its stress increment tensor, defined as

$$\Delta\tau = \tau_f - \tau_i, \quad (3)$$

where  $\tau_i$  denotes the system stress tensor at onset and  $\tau_f$  at completion of the relaxation. The pressure and deviatoric components of  $\Delta\tau$  associated with the 4201 observed events can be computed as described in Sec. II. The pressure components of the stress relaxation increment tensors

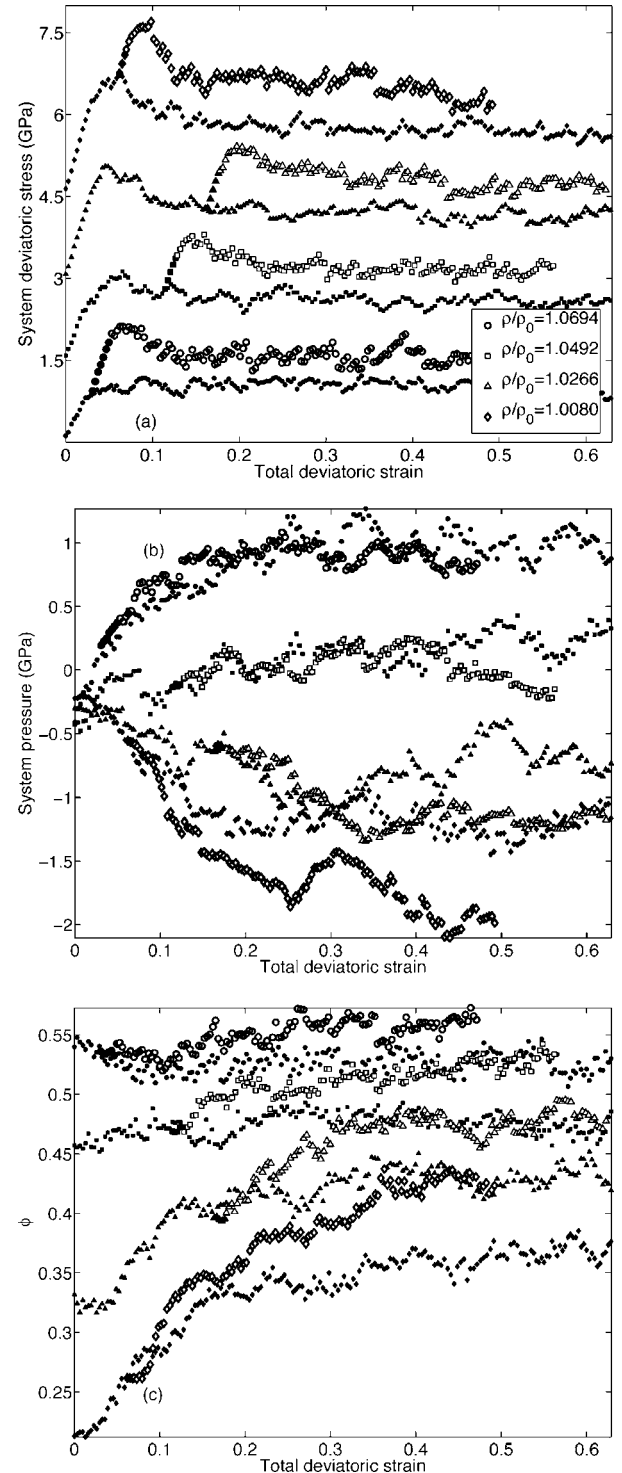


FIG. 1. These figures show the variations of (a) the deviatoric stress  $\bar{\sigma}(\tau)$ , (b) pressure  $p(\tau)$ , and (c) mass fraction of liquidlike atomic environments  $\phi$  as functions of total externally applied deviatoric strain  $\bar{\epsilon}(\epsilon)$  for four a-Si systems of differing densities undergoing large-strain plastic flow under constant volume. Variations in  $p(\tau)$  and  $\phi$  show similar trends for both PEM simulations (large markers) and MD at  $T=300$  K (Refs. 1 and 2) (small markers) while  $\bar{\sigma}(\tau)$  is elevated in the PEM case. The data series in (a) all begin at the origin, but have been offset in increments of 1.5 GPa for clarity.

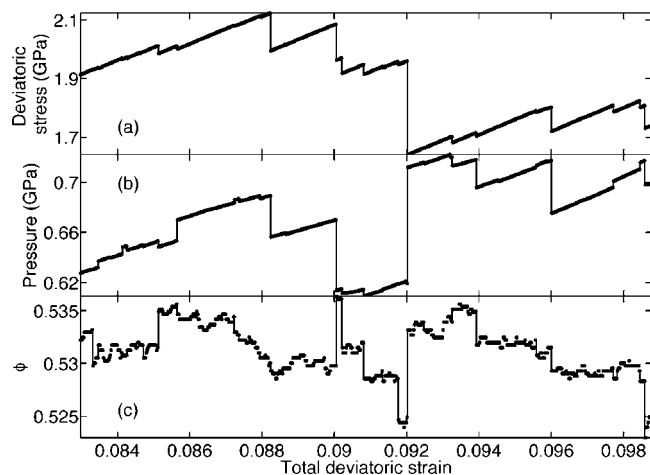


FIG. 2. Variations of (a) deviatoric stress  $\bar{\sigma}(\tau)$ , (b) pressure  $p(\tau)$ , and (c) mass fraction of liquidlike atomic environments  $\phi$  as functions of total externally applied deviatoric strain  $\bar{\epsilon}(\epsilon)$  over a typical section of a PEM plastic deformation simulation are shown above. The stress-strain plots are composed of regions of smooth reversible deformation (denoted by dots) punctuated by discrete irreversible stress relaxations (vertical lines), each occurring at a well-defined threshold stress. The largest changes in  $\phi$  coincide with the largest stress relaxations. Nevertheless, some fluctuations in  $\phi$  do occur in regions of reversible stress variation. Data for this figure were obtained by enlarging the plots shown in Figs. 1(a)–1(c) for the a-Si system with  $\rho/\rho_0=1.0694$  in the range of total deviatoric strain presented above.

were distributed symmetrically about zero. The normalized distribution of their absolute values can be described as a power law with the approximate form  $0.0141(|p(\Delta\tau)|/37.76 \text{ GPa})^{(-1.28\pm 0.05)}$ . The normalized distribution of deviatoric stress-relaxation increments can be described as a power law with the approximate form  $0.0162(\bar{\sigma}(\Delta\tau)/37.76 \text{ GPa})^{(-1.29\pm 0.04)}$ . Here 37.76 GPa is the approximate decohesion stress for SW Si obtained by dimensional analysis from the characteristic energy and length of the SW potential.<sup>11</sup>

The intensity of internal structure change accompanying every stress relaxation can be additionally characterized by the number of atomic environments whose character changed during the relaxation from liquidlike to solidlike or vice versa. This quantity will be called  $\chi$ . Although the pressure increments  $p(\Delta\tau)$  and  $\chi$  show no recognizable correlation, the deviatoric stress increments  $\bar{\sigma}(\Delta\tau)$  and  $\chi$  are directly correlated as shown in Fig. 3. This finding indicates that, in amorphous Si, every unit of stress relaxation is accompanied by a characteristic increment of internal structure change. Furthermore, since the number of environment changes only correlates to the deviatoric stress increment and not the pressure increment, it can be concluded that internal structure changes in a-Si during discrete stress relaxations are shear-induced.

No correlation was found between the mechanical threshold stress  $\tau_i$  at onset of relaxations and  $p(\Delta\tau)$ ,  $\bar{\sigma}(\Delta\tau)$ , or  $\chi$ . The intimate details of structure changes that accompany discrete stress relaxations, however, are a means of studying the mechanisms of plastic flow in a-Si, whereas the conditions at

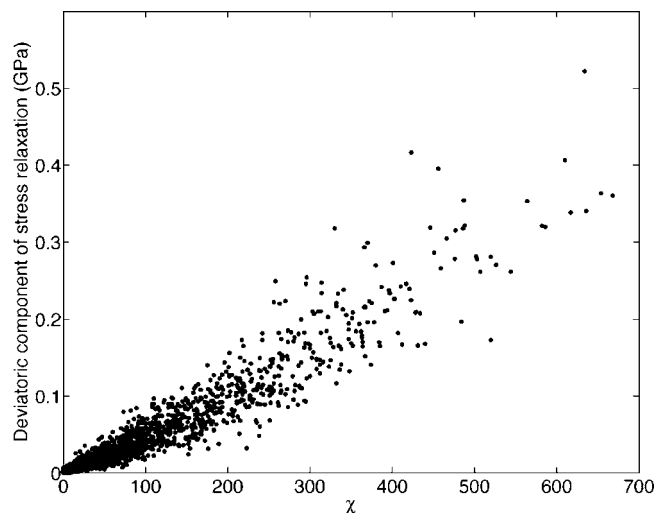


FIG. 3. The number  $\chi$  of atomic environments whose character changes during a stress relaxation (from liquidlike to solidlike or vice versa) is directly correlated to its deviatoric component  $\bar{\sigma}(\Delta\tau)$ .

the mechanical thresholds preceding these relaxations can elucidate the local yielding criteria at onset of atomic rearrangements. These mechanisms and onset conditions are analyzed in detail in the following sections.

## V. IDENTIFICATION OF REGIONS TRANSFORMING INELASTICALLY DURING STRESS RELAXATIONS

Every discrete stress relaxation event in PEM deformation simulations is accompanied by an internal structure rearrangement accomplished through the relative displacements of atoms. Some of these relative position changes are large and indicate a local inelastic transformation of atomic structure. Others are small and can be considered elastic. Consequently, the overall behavior of an a-Si system undergoing stress relaxation can be viewed as the composite response of an inelastically transforming inclusion and an elastically deforming matrix that surrounds the inclusion, much like in the case of martensitic shear transformations. To identify the part of an a-Si system that undergoes an inelastic atomic structure transformation during a stress relaxation means simply to distinguish between the part whose deformation can be described as approximately elastic and the part whose deformation cannot be described in that way. The elastically deforming part of the system is identified as matrix material and is expected to be primarily outside the transforming cluster. The complement to the elastically deforming part is called the inelastically transforming inclusion. This description of the composite response of a system to a localized inelastic structure transformation is the same as the basic setting of Eshelby's inclusion problem.<sup>37</sup>

Previous studies have observed that structure rearrangements accompanying stress relaxations are clustered into well-localized regions and can involve relatively few<sup>6,38,39</sup> or many<sup>32,36</sup> participating atoms, depending on the bonding and size of the system under consideration as well as the loading conditions. Many of these studies identified the regions undergoing structure transformations by making use of strain

measures appropriately generalized to individual atomic environments<sup>40–42</sup> to locate centers of high-intensity non-affine atomic displacements. Because strain measures by themselves do not differentiate between plastic strains occurring in a transforming inclusion and compatibility-induced elastic strains in the surrounding matrix, however, this approach ignores the physical basis for making the matrix-inclusion distinction. As a result, strain measure techniques can identify elastically deforming material in the proximity of an inelastically transforming inclusion as part of that inclusion simply because the elastic strains there are large. This study uses a method that makes no recourse to strain measures for recognizing inelastically transforming inclusions.

Intuitively, a material is understood to behave elastically if increments in its state of deformation produce increments of the corresponding forces in linear (or nearly linear) proportion to the deformation increments themselves. In a continuum setting, this intuition can be stated as the linear dependence of stresses on strain increments

$$\boldsymbol{\tau}_f = \boldsymbol{\tau}_i + \mathbf{C}(\boldsymbol{\Delta}\boldsymbol{\varepsilon}). \quad (4)$$

Here  $\boldsymbol{\tau}_f$  and  $\boldsymbol{\tau}_i$  are the final and initial stress states,  $\boldsymbol{\Delta}\boldsymbol{\varepsilon}$  is a strain increment tensor, and  $\mathbf{C}$  is the tensor of linear elastic constants. In an atomistic setting, however, all degrees of freedom are discrete, making the determination of physically meaningful atomic-site strain increments and elastic constants inconvenient. It is far more expedient to restate the intuitive relation in Eq. (4) using quantities that are more natural in the discrete atomic setting. Consider two configurations—initial and final—of an atomic system under periodic boundary conditions. If the atomic positions in these configurations differ, but the shapes of their simulation cells are identical, then Eq. (4) can be restated as

$$\mathbf{f}_f = \mathbf{f}_i + (-\mathbf{H}) \cdot (\boldsymbol{\Delta}\mathbf{d}). \quad (5)$$

In expression (5) the force vectors  $\mathbf{f}_f$  and  $\mathbf{f}_i$  take the place of final and initial stress states, relative displacements  $\boldsymbol{\Delta}\mathbf{d}$  play the role of the strain increment tensor, and the negative of the Hessian matrix  $\mathbf{H}$  (i.e., the matrix of second derivatives of the system potential with respect to atomic positions) plays the role of the elastic constants. More generally, if in addition to having different atomic positions, the two atomic configurations also have simulation cells whose shapes differ by a strain increment tensor  $\boldsymbol{\Delta}\boldsymbol{\varepsilon}$ , then Eq. (5) can be restated as

$$\mathbf{f}_f = \mathbf{f}_i + (-\mathbf{H}) \cdot (\boldsymbol{\Delta}\mathbf{d}) + \frac{\partial \mathbf{f}_i}{\partial \varepsilon_{ab}} \cdot \Delta \varepsilon_{ab}. \quad (6)$$

The quantities  $\partial \mathbf{f}_i / \partial \varepsilon_{ab}$  are the direct variations of forces on atoms  $\mathbf{f}_i$  with variations in the strain components  $\varepsilon_{ab}$ . These force variations are calculable analytically as derivatives of the total system potential, much like the components of  $\mathbf{H}$ . The quantities  $\Delta \varepsilon_{ab}$  are the components of the strain increment tensor  $\boldsymbol{\Delta}\boldsymbol{\varepsilon}$ . Summation over repeated indices is implied. For a system in three dimensions consisting of  $N$  atoms, the force, displacement, and force variation vectors ( $\mathbf{f}_f, \mathbf{f}_i, \boldsymbol{\Delta}\mathbf{d}, \partial \mathbf{f}_i / \partial \varepsilon_{ab}$ ) in Eq. (6) have  $3N$  components while the Hessian matrix  $\mathbf{H}$  has  $3N \times 3N$  components.

If a system undergoes a deformation that is not purely linear elastic, then the total forces on individual atoms in its final configuration can be decomposed into a linear elastic contribution, calculable by Eq. (6), and some excess force increment  $\boldsymbol{\Delta}\mathbf{f}$

$$\mathbf{f}_f^{\text{total}} = \mathbf{f}_f^{\text{elastic}} + \boldsymbol{\Delta}\mathbf{f}. \quad (7)$$

Identifying  $\mathbf{f}_f^{\text{elastic}}$  with  $\mathbf{f}_f$  in expression (6), the force deviation  $\boldsymbol{\Delta}\mathbf{f}$  can be expressed as

$$\boldsymbol{\Delta}\mathbf{f} = \mathbf{f}_f^{\text{total}} - \mathbf{f}_f^{\text{elastic}} = (\mathbf{f}_f^{\text{total}} - \mathbf{f}_i) + \mathbf{H} \cdot (\boldsymbol{\Delta}\mathbf{d}) - \frac{\partial \mathbf{f}_i}{\partial \varepsilon_{ab}} \cdot \Delta \varepsilon_{ab}. \quad (8)$$

The final forces on atoms in a discrete system that has undergone purely linear elastic deformation would be exactly predicted by Eq. (6). By construction the force deviation  $\boldsymbol{\Delta}\mathbf{f}$  computed for such a case using expression (8) would therefore be zero. It would be nonzero for a system that underwent deformation that was not purely linear elastic.

Thus far, the force deviation  $\boldsymbol{\Delta}\mathbf{f}$  for a deforming system was considered as a complete  $3N$ -component vector. If the components of the force deviation vector are considered separately, however, they can be used to distinguish between a linear elastically deforming matrix and inelastically transforming inclusion. If the environment of an atom undergoes an essentially linear elastic deformation, the three components ( $x$ ,  $y$ , and  $z$ ) of the force deviation  $\boldsymbol{\Delta}\mathbf{f}$  corresponding to that atom will be nearly zero. Meanwhile, if the atomic environment in question deforms in a way that departs strongly from linear elasticity, these force deviation components will be large. For the environment of any atom  $k$ , therefore, a measure of deviation from linear elastic deformation can be defined as

$$\delta_k = \frac{\sqrt{(\boldsymbol{\Delta}\mathbf{f})_{k,x}^2 + (\boldsymbol{\Delta}\mathbf{f})_{k,y}^2 + (\boldsymbol{\Delta}\mathbf{f})_{k,z}^2}}{|\boldsymbol{\Delta}\mathbf{f}|}, \quad (9)$$

where  $(\boldsymbol{\Delta}\mathbf{f})_{k,x}$  is the  $x$  component on atom  $k$  of the complete force deviation vector  $\boldsymbol{\Delta}\mathbf{f}$  and

$$|\boldsymbol{\Delta}\mathbf{f}| = \sqrt{\sum_{a=1}^{3N} (\boldsymbol{\Delta}\mathbf{f})_a^2}$$

is simply the norm of  $\boldsymbol{\Delta}\mathbf{f}$ . Once calculated, the atomic measures of deviation from linear elasticity  $\delta_k$  are sorted in descending order. In this study, sorting was performed using the SLATEC implementation of DPSORT<sup>43</sup> (available on Netlib<sup>25</sup>). Then the number  $n$  of atoms in an inelastically transforming inclusion is defined by

$$\sqrt{\sum_{j=1}^n \delta_{k(j)}^2} > 0.95, \quad (10)$$

where  $k(j)$  denotes the atom  $k$  corresponding to the  $j$ th position in the sorted queue of deviation measures  $\delta_k$ .

In other words, the procedure above identifies the environments of atoms with  $\delta_k \approx 0$  as undergoing linear elastic deformation and therefore considers them part of the elastically deforming matrix. The inelastically transforming inclusion is the complement of the elastically deforming matrix. It

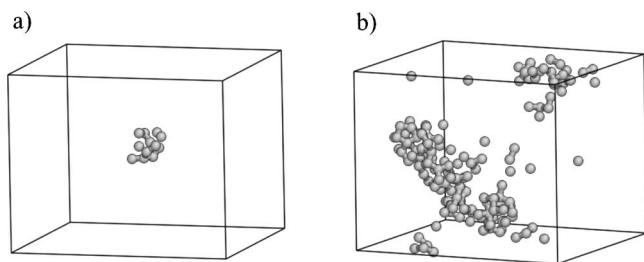


FIG. 4. Visualizations of two typical inelastically transforming inclusions: one consisting of 12 atoms in a single cluster (a), the other of 154 atoms grouped mainly into two separate clusters (b).

is composed of the smallest number of atoms necessary to account for at least 95% of the norm of the force deviation vector  $\Delta \mathbf{f}$ . The fact that  $n$  is indeed the smallest number of atoms necessary to do so is assured by counting the atoms with the largest contribution to the norm of the force deviation first in the summation in Eq. (10). The specific atoms forming the inclusion are simply the first  $n$  atoms from the sorted queue  $k(j)$ . The atoms comprising the elastically deforming matrix are then the remaining  $(N-n)$  atoms in the queue. It should be emphasized that the distinction between matrix and inclusion based on the above analysis is inherently approximate. In particular, the cutoff in Eq. (10) can be chosen larger or smaller, yielding more or less conservative estimates of the extent of inelastically transforming inclusions, respectively. It has been found, however, that the conclusions from the analyses to be presented below are unaffected by varying this cutoff between 0.90 and 0.99, indicating that they are robust with respect to the chosen level of approximation.

The method described above was used to identify and analyze the inelastically transforming inclusions associated with the 4201 discrete stress-relaxation events observed in the course of PEM deformation simulations (Sec. III). The atomic arrangements at the mechanical thresholds (just before relaxation) and at completion of the ensuing stress relaxations served as initial and final system configurations, respectively. Both configurations are by construction in equilibrium, so  $\mathbf{f}_i = \mathbf{f}_f^{\text{total}} = 0$  in Eq. (8). Furthermore, the shapes of their simulation cells differ by  $\Delta \boldsymbol{\varepsilon}$  equal to one externally applied volume-conserving system strain increment, as described in Sec. II. Figure 4 shows visualizations of two representative transforming inclusions found by the matrix-inclusion analysis. One of them [Fig. 4(a)] is composed of 12 atoms grouped into one cluster. The other one [Fig. 4(b)] is larger at 154 atoms and appears to consist primarily of two separate atomic clusters (and a handful of isolated atoms). The atomic clusters observed in both inclusions are well localized, as can be concluded by observing that they are confined to relatively compact regions within the simulation cell.

## VI. INELASTIC TRANSFORMATIONS AS AUTOCATALYTIC AVALANCHES OF UNIT SHEARING EVENTS

The sizes of the 4201 inelastically transforming inclusions, defined as the number  $n$  of atoms composing each one,

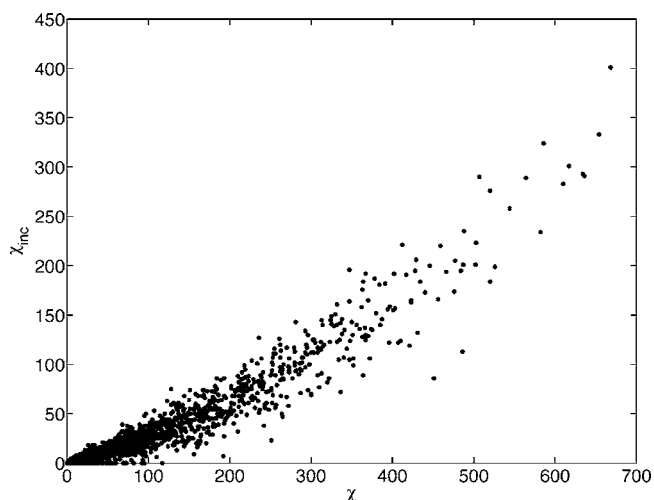


FIG. 5. The numbers  $\chi_{\text{inc}}$  of atomic environment transitions (from liquidlike to solidlike and vice versa) that take place within the nearest-neighbor shells of atoms comprising inelastically transforming inclusions are plotted against the total numbers  $\chi$  occurring during stress relaxations. It can be concluded that about 40% of such transitions occur due to inelastic transformation and the rest due to elastic flexing.

were distributed according to a power law of approximate form  $7.64 \times n^{(-1.96 \pm 0.09)}$  and ranged between 3 and just over 600 atoms. Meanwhile, Fig. 3 shows that the number  $\chi$  of atomic environment changes during stress relaxations reaches a maximum of almost 700. This observation prompts an investigation of whether all transitions of atomic environments between the solidlike and liquidlike types occur as a result of inelastic rearrangement or if some of them are caused by flexing of bond angles in the elastically deforming matrix, as suggested in Sec. III. The exact proportion of atomic environment transitions taking place elastically and inelastically can be found by plotting the number  $\chi_{\text{inc}}$  of such transitions taking place within the nearest-neighbor shells of atoms comprising inelastically transforming inclusions against the total number  $\chi$  occurring during stress relaxations, as shown in Fig. 5. From the slope of the trend, it can be discerned that about 40% of such transitions occur due to inelastic transformation and the rest due to elastic flexing. This conclusion is not materially affected by varying the cutoff chosen in Eq. (10) for finding the atoms comprising inelastically transforming inclusions. Figure 6 visualizes the location of atomic environments that undergo a change in their type and are not in the nearest-neighbor shells of atoms comprising the inelastically transforming inclusion for the two inclusions shown in Fig. 4.

More importantly, however, the sizes of transforming inclusions  $n$  exhibited a similar correlation to the pressure and deviatoric components of the stress-relaxation tensor  $p(\Delta \boldsymbol{\tau})$  and  $\bar{\sigma}(\Delta \boldsymbol{\tau})$ , as did the number  $\chi$  of atomic environment changes during the stress relaxations (Fig. 3). Specifically,  $p(\Delta \boldsymbol{\tau})$  and  $n$  show no recognizable correlation. Meanwhile, Fig. 7 demonstrates that  $\bar{\sigma}(\Delta \boldsymbol{\tau})$  and  $n$  are roughly linearly related, suggesting there exists for amorphous Si a characteristic increment of stress relaxation per unit volume, i.e., a “unit” inelastic deformation event. Furthermore, since inclu-

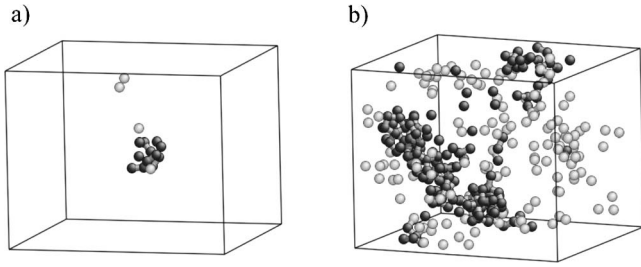


FIG. 6. Visualizations of atomic environment transitions for the two typical inelastically transforming inclusions exhibited in Fig. 4. The dark atoms are those that constitute the inelastically transforming inclusions themselves. The light atoms denote environments that changed their type (from liquidlike to solidlike or vice versa), but are not part of the nearest-neighbor shells of the atoms that constitute the inclusions.

sion sizes only correlate to the deviatoric component of stress increments and not the pressure component, such a unit event can be characterized as a shear transformation with an uncorrelated dilatational component.

This conclusion is further reinforced by examination of the evolution of the transforming inclusions during the process of structure relaxation (carried out by potential energy minimization, as described in Sec. II). This process begins just beyond mechanical threshold of a given stress relaxation, proceeds in an unconstrained manner through a series of nonequilibrium states, and ends with the eventual system-wide equilibration of the atomic configuration in a local potential-energy minimum. Because it does not take account of inertial effects, this method of examining stress relaxations only yields information concerning the chronological ordering of events leading to the growth of transforming inclusions and not the relative time scales on which these events occur. Such examination is carried out for the two representative transforming inclusions visualized in Figs. 4 and 6. The progress of the relaxation procedure is gauged by finding the norm of the vector of atomic displacements  $\Delta\mathbf{d}$  from the reference configuration at the beginning of the re-

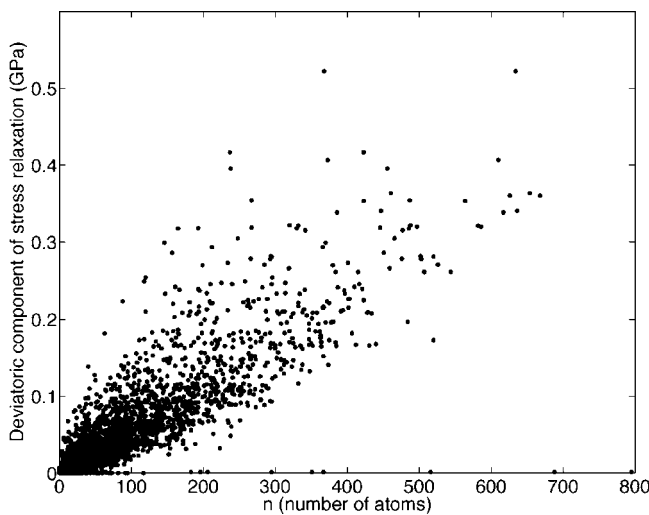


FIG. 7. The deviatoric component  $\bar{\sigma}(\Delta\tau)$  is roughly linearly related to the inclusion size  $n$ .

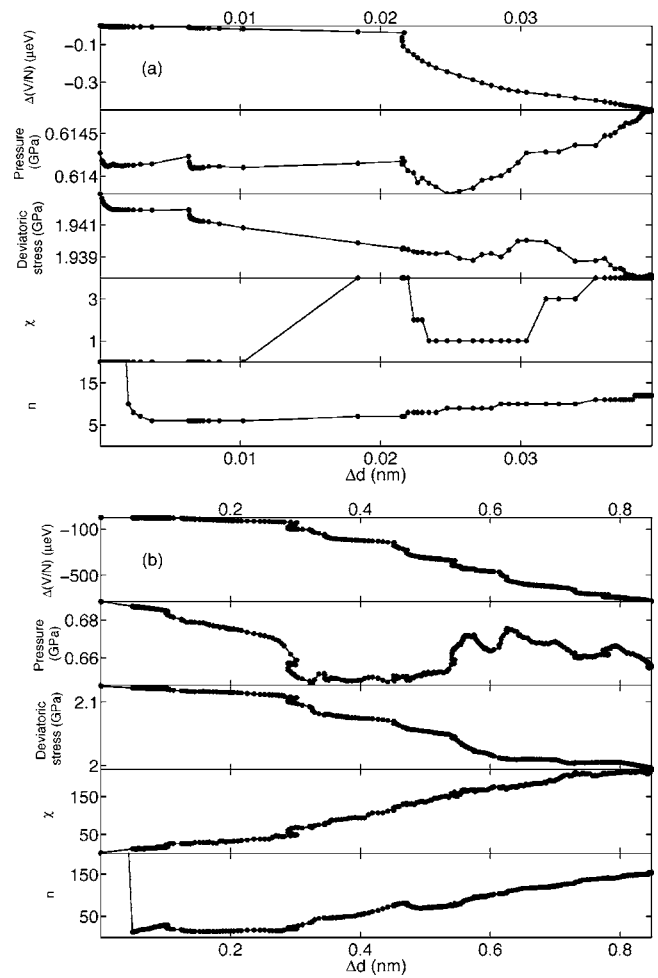


FIG. 8. The variations of system potential-energy increment per atom  $\Delta(V/N)$ , system pressure  $p(\tau)$ , and deviatoric stress  $\bar{\sigma}(\tau)$ , number of atomic environment changes  $\chi$ , as well as size  $n$  of the inelastically transforming inclusion as functions of the norm of the atomic displacement vector  $|\Delta\mathbf{d}|$  for (a) the small relaxation visualized in Figs. 4(a) and (b) the large relaxation visualized in Fig. 4(b).

laxation to the current configuration at any given stage of the relaxation. The increasing size of the inelastically transforming inclusion is monitored at every step of the relaxation process using the matrix-inclusion analysis described in Sec. V with the system configuration at the mechanical threshold as a reference state. Quantities such as potential energy, system pressure, and deviatoric stress, as well as total number  $\chi$  of atomic environment transitions are also monitored.

Figure 8(a) shows that the inelastic transformation of the small inclusion visualized in Figs. 4(a) and 6(a) proceeds in a single spurt associated with a sudden decrease in system potential energy and deviatoric stress as well as an increase in inclusion size and the total number of atomic environments that underwent structure transitions. Figure 8(b) demonstrates that similar intermittent spurts occur during the inelastic transformation of the larger inclusion. In both cases, the system deviatoric stress is progressively relaxed as the extent of elastically transformed material increases, confirming the hypothesis of a characteristic increment of shear stress relaxation per unit volume of transformed material.

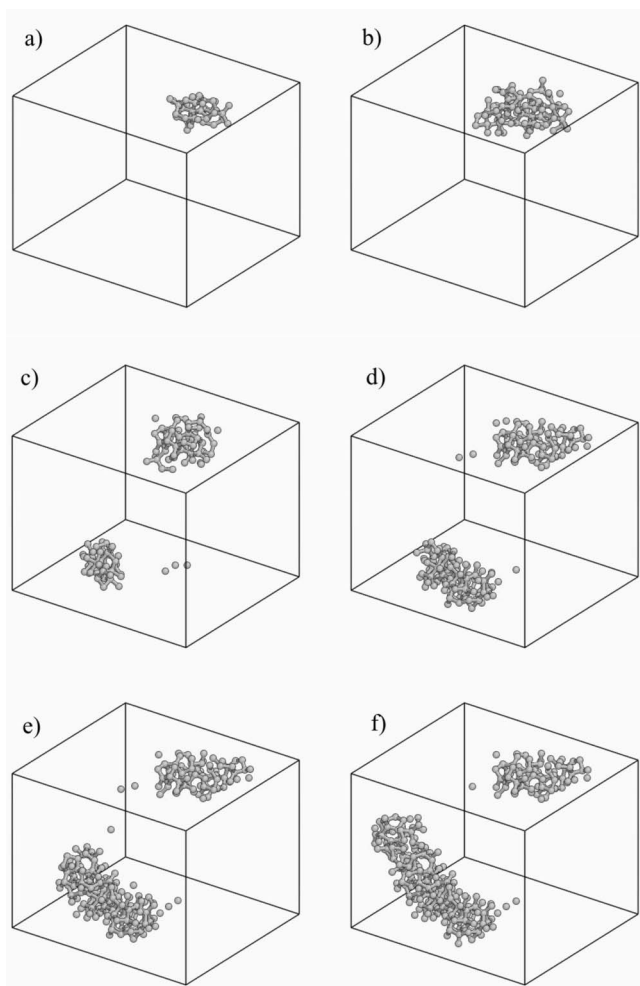


FIG. 9. Visualizations of the evolution of the inelastically transforming inclusion shown in Fig. 4(b) and analyzed in Fig. 8(b). The norms of the atomic displacement vector  $|\Delta\mathbf{d}|$  in each frame are (a) 0.049 nm, (b) 0.103 nm, (c) 0.392 nm, (d) 0.593 nm, (e) 0.629 nm, and (f) 0.705 nm.

Furthermore, visualizations (in Fig. 9) of the aggregation of inelastically transformed regions in the case of the larger of the two inclusions indicate that successive transformation generally occurs in the vicinity of previously transformed material. This observation suggests that inelastic relaxation in a-Si is an autocatalytic avalanche of unit shear relaxations that continues as long as a local yielding criterion is satisfied. Since inelastic relaxation can change the local distribution of stresses and cause elastically induced changes in the type of atomic environments throughout the neighboring matrix material, inelastic transformations can also initiate in atomic clusters that are close to but disconnected from the body of the cluster that originally underwent inelastic transformation. The details of the local yielding phenomenon responsible for the local onset of inelastic transformation are investigated next.

### VII. TRIGGERING INCLUSIONS AS A MEANS OF STUDYING LOCALIZED YIELDING IN a-Si

One way to investigate the character of the local yielding condition proposed in Sec. VI is to recognize that each of the

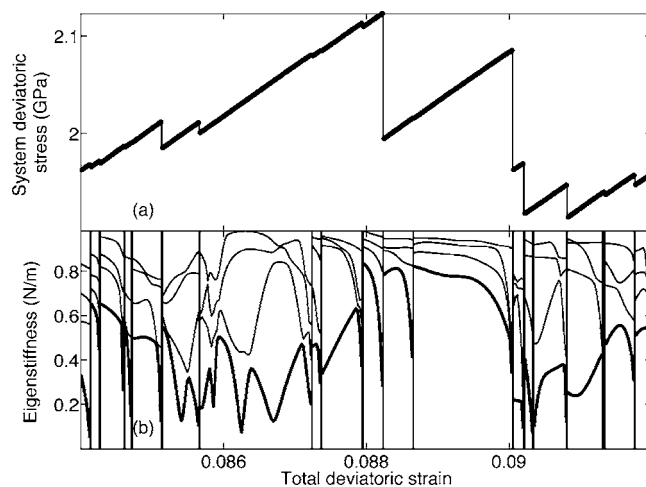


FIG. 10. The onset of every discrete stress relaxation is accompanied by the vanishing of the stiffness of one of the normal modes of the complete Hessian matrix for the a-Si system. Data for this figure were obtained from PEM deformation of the a-Si system with  $\rho/\rho_0=1.0694$  in the range of total deviatoric stress presented above.

autocatalytic avalanches of unit events that account for the observed stress relaxations must have been initiated or “triggered” when such a condition was satisfied. It should therefore be possible to find the characteristics of local yielding by investigating the onset of discrete relaxations. In agreement with previous findings in model metallic glasses,<sup>39,44</sup> the onset of each discrete relaxation was accompanied by the vanishing of the stiffness of one of the normal modes of the complete Hessian matrix for the a-Si system, as illustrated in Fig. 10 (the method of finding these stiffnesses was described in Sec. II). This “soft-mode” phenomenon is characteristic of steady-state bifurcations of equilibrium paths<sup>45,46</sup> and plays an important role in the study of ferroelectric and antiferroelectric phase transitions<sup>47</sup> as well as martensitic transformations.<sup>48</sup> Figure 11 shows that the decrease of successive normal-mode stiffnesses below zero and their eventual increase back toward positive values also accompanies the progress of inelastic transformations themselves. The consecutive vanishing of these normal-mode stiffnesses corresponds to the repetitive onset of local yielding during the autocatalytic avalanches of unit events in the a-Si systems after the initial triggering of a stress relaxation. These successive onset phenomena could also serve as a basis for the study of local yielding in a-Si, but it is easier to only consider the initial triggering of stress relaxations instead.

The nature of the steady-state bifurcations accompanying triggering of stress relaxations can be ascertained by evaluating two derivatives of the potential energy of the complete a-Si system at the mechanical threshold stress. The first is  $V'_1$ , the mixed derivative of the potential energy with respect to displacements along the normal mode of vanishing stiffness or “critical eigenmode” [(CE), indicated by subscript 1] and externally applied strain increment value (Sec. II, indicated by prime). The second is  $V_{111}$ , the third derivative of the system potential energy with respect to displacements along the CE. In particular, if both  $V'_1$  and  $V_{111}$  are nonzero, the bifurcation is of the saddle-node type and describes the van-

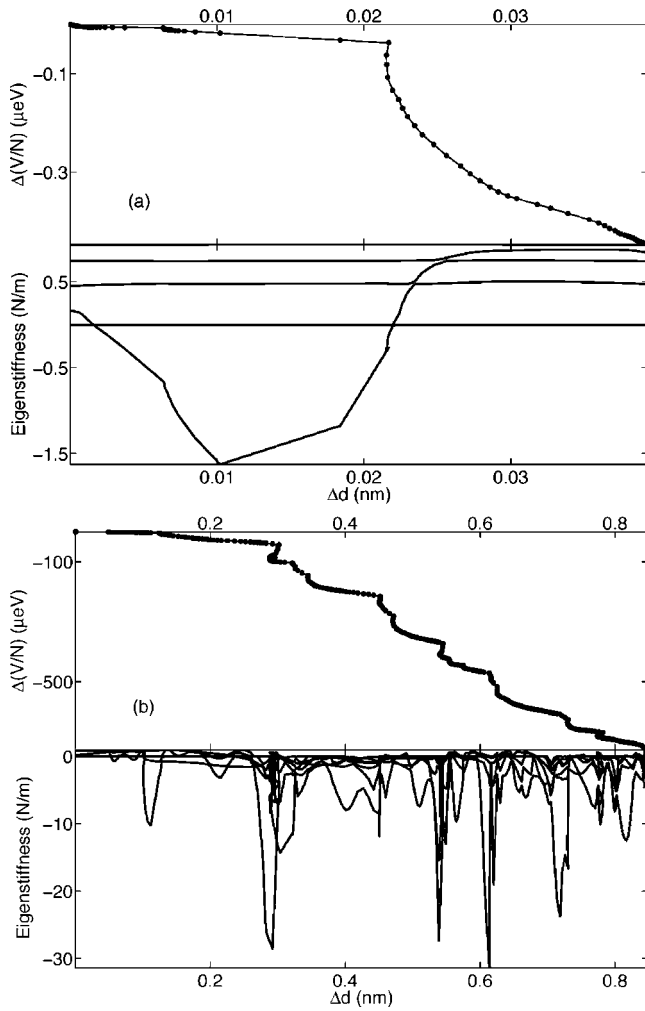


FIG. 11. The decrease of successive normal-mode stiffnesses below zero and their eventual increase back toward positive values accompanies the progress of inelastic transformations. Here, (a) and (b) correspond to the small and large relaxations, respectively, analyzed in Fig. 8 and visualized in Fig. 4.

ishing of a stable equilibrium path as it merges with an unstable equilibrium path. The sudden and irreversible relaxation of stress in a system that has been strained infinitesimally beyond its mechanical threshold is a direct consequence of the finite atomic displacements necessary for the system to attain some distant stable equilibrium configuration following the vanishing of the original stable equilibrium path at the point of bifurcation. This type of behavior is often called “snapping” in the study of elastic stability.<sup>49</sup>

All 4201 stress relaxations observed in the PEM deformation simulations described in Secs. II–IV satisfied the conditions  $V'_1 \neq 0$  and  $V_{111} \neq 0$  at their onset, confirming that they were all triggered by a process describable as a saddle-node bifurcation. This result is to be expected since saddle-node bifurcations typically occur in systems lacking in any intrinsic symmetry or equilibrium configurations.<sup>45,46</sup> Unlike crystal lattices, whose intrinsic symmetries induce bifurcations more complex than those of the saddle-node type,<sup>50</sup> a-Si—much like other atomically disordered solids—does not have any structural symmetry properties. Interestingly, this lack of

intrinsic ordering has a simplifying effect on the analysis of the onset of stress relaxations in a-Si insofar as it explains the exclusive occurrence of saddle-node bifurcations during deformation.

In Sec. V, it was shown that knowledge of the finite atomic displacements accompanying stress relaxations can be used to distinguish between elastically deforming matrix material and an inelastically transforming inclusion in the case of each relaxation. A similar analysis can be carried out at the mechanical threshold preceding a stress relaxation to find a “triggering inclusion” where local yielding of strained material initiates. Unlike the transformation process associated with stress relaxations, however, triggering is described not by finite displacements of atoms but rather by the infinitesimal variations in their positions included in the CE. The framework for distinguishing between matrix and inclusion material described in Sec. V can still be applied if the total forces in the “final” configuration [Eq. (7)] are expressed as a Taylor expansion around the initial configuration:

$$\mathbf{f}_f^{\text{total}} = \mathbf{f}_i + (-\mathbf{H}) \cdot \mathbf{d} + \frac{1}{2}(-\mathbf{t}) + \dots \quad (11)$$

Here  $\mathbf{d}$  is the  $3N$ -component vector of displacement increments and  $\mathbf{H}$  the Hessian (matrix of second derivatives of the system potential energy with respect to these displacements), as before.  $\mathbf{t}$  is the quadratic contribution to the expansion in Eq. (11). It is a vector quantity that depends on the third derivatives of the system potential energy with respect to displacement as

$$t_k = \frac{\partial^3 V}{\partial x_a \partial x_b \partial x_k} d_a d_b \quad (12)$$

where  $t_k$  is the  $k$ th component of the vector  $\mathbf{t}$  and  $d_a$  is the  $a$ th component of the displacement increment vector  $\mathbf{d}$ . There is no contribution in Eq. (11) from terms of the type  $\partial \mathbf{f}_i / \partial \varepsilon_{ab}$  [unlike in Eq. (6)] because triggering is assumed to occur at a fixed shape of the simulation cell. Summation over repeated indices is implied in both Eqs. (11) and (12).

Applying the definition in Eq. (8) to the description of force variations during triggering in Eq. (11) gives

$$\Delta \mathbf{f} \approx -\frac{1}{2} \mathbf{t} \quad (13)$$

if the expansion for forces in Eq. (11) is truncated after the quadratic term.

In the case of the CE, which describes the kinematics of triggering, the vector of infinitesimal displacement increments can be written

$$\mathbf{d} = s \hat{\mathbf{e}}, \quad (14)$$

where  $\hat{\mathbf{e}}$  is the unit CE vector and  $s$  is a scalar displacement parameter. Equations (13) and (14) therefore give

$$(\Delta \mathbf{f})_k \approx -s^2 \frac{\partial^3 V}{\partial x_a \partial x_b \partial x_k} e_a e_b = -s^2 V_{11k}, \quad (15)$$

where  $-V_{11k}$  are the components of the vector of second derivatives of forces on individual atoms with respect to displacements along the CE (denoted by subscript 1, as before). Knowing the shape of the CE,  $V_{11k}$  can be determined analytically from the form of the empirical potential governing

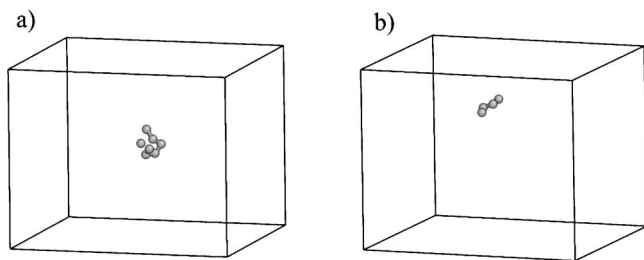


FIG. 12. The triggering clusters found at onset of the stress relaxations associated with the transforming inclusions visualized in Fig. 4. Cluster (a) consists of seven atoms while (b) consists of four.

the system. Alternatively, they can also be found by evaluating numerically the second derivatives of forces on atoms along the CE. The latter method was used in this study.

The force deviations in Eq. (15) describe the departure from the predictions of linear elasticity in the case of the infinitesimal displacements associated with triggering. They can be used in conjunction with Eqs. (9) and (10) to define a triggering cluster for the onset of every stress-relaxation event. These clusters are always localized in the vicinity of atomic sites that undergo the largest relative displacements, as quantified by the components of the unit CE vector  $\hat{e}$ . The degree of localization exhibited by  $V_{11k}$ , however, is always significantly greater than that exhibited by  $\hat{e}$  because the latter, in addition to containing information about the atomic cluster undergoing localized yielding, also characterizes the compatibility-induced elastic flexing of the surrounding matrix material.

In light of the above development, a clear distinction must be made between these triggering clusters and the inelastically transforming inclusions defined in Sec. V. The latter characterizes a finite and irreversible atomic rearrangement, whereas the former merely probes nonlinear departures from linear elastic behavior under infinitesimal displacement, in particular their spatial localization. These departures, however, carry a specific meaning in the case of triggering of stress relaxations. At the mechanical threshold, the component of the return force against displacements along the CE that is linear in those displacements vanishes and the system can undergo a finite atomic rearrangement given even an infinitesimal increment in loading. The largest of the deviations from linear elasticity  $V_{i11}$  in this situation specify the fastest growing force components that initiate this finite atomic rearrangement. The atomic sites with the highest measure of deviation from linear elasticity  $\delta_k$  [Eq. (9)] indicate the location where it nucleates.

Figure 12 shows the triggering clusters found by the above analysis at the mechanical thresholds associated with the transforming inclusions visualized in Figs. 4 and 6. The triggering clusters are compact and well localized. They consist of 7 and 4 atoms, whereas the corresponding transforming inclusions contain 12 and 154 constituent atoms, respectively. By investigating the onset of the 4201 stress relaxations found in this study, it was determined that triggering cluster sizes are distributed exponentially with an average of  $7.0 \pm 5.2$  atoms per inclusion. Furthermore, the sizes of these clusters are not correlated to the components of the

ensuing stress-relaxation increments or the sizes of the associated transforming inclusions, suggesting that all irreversible stress relaxations, regardless of their magnitude, are triggered in the same way on average.

To determine the local yielding criterion leading to the onset of stress relaxations, the total stress tensor characterizing the environment of each triggering cluster is found. This determination is accomplished by summing up the individual atomic stress tensors (Sec. II) of all atoms in the triggering cluster along with their nearest neighbors. The pressure and deviatoric components of this stress tensor  $p(\Delta\tau)$  and  $\bar{\sigma}(\Delta\tau)$  are obtained. The mass fraction  $\phi$  of liquidlike material in the clusters is also calculated. In about 8.7% of all cases, it is found that the triggering cluster consists of two or three distinct atomic subclusters. In such situations, both the stress state and  $\phi$  are determined separately for each subcluster.

Figure 13 plots average values of the cluster deviatoric stress as a function of the cluster pressure and  $\phi$ . A clear quadratic dependence of the deviatoric stress on both quantities confirms the existence of a well-defined microyield surface. As expected,<sup>1,2</sup> [Fig. 13(a)] confirms that an increasing  $\phi$  results in a declining yield stress. It also shows, however, that for high-enough  $\phi$  this trend reverses and an increasing yield stress is observed. The minimum yield stress occurs at about  $\phi=0.6$ . Figure 13(b) shows that the dependence of yield stress on pressure is relatively less pronounced than the dependence on  $\phi$ . Minimum yield stresses are achieved at about zero pressure.

The presence of the well-defined local yielding criterion shown in Fig. 13 explains why the analyses presented in this study always give the same results regardless of whether the stress relaxations in each deformation run are considered separately or as one set of 4201 events (as claimed in Sec. IV). In short, since the properties that govern the relaxations are the local properties that enter into the local yielding criterion, the overall system pressure, deviatoric stress, and liquidlike mass fractions are irrelevant.

According to the analysis in Sec. VI, inelastic transformations in a-Si proceed as autocatalytic avalanches of unit inelastic shearing events as long as the local yielding criterion presented in Fig. 13 is satisfied at some location in the system. The nature of the unit events comprising these avalanches is clarified in Sec. VIII.

### VIII. RECURRING ATOMIC BONDING CHANGES IN TRIGGERING CLUSTERS

It was argued in Secs. VI and VII that there exists a unit inelastic structure transformation characteristic of a-Si that is responsible for stress relaxations as well as their initial triggering. Simple inspection of the structure of triggering clusters (Fig. 12) and subsequent inelastically transforming inclusions (Fig. 4), however, revealed no such readily identifiable atomic rearrangement. Information concerning recurring structural and kinematical features at onset of stress relaxations can nevertheless be obtained by evaluating combined distribution functions over all 4201 triggering clusters.

Bond lengths characteristic of triggering clusters were found by compiling a histogram of all the collected inter-

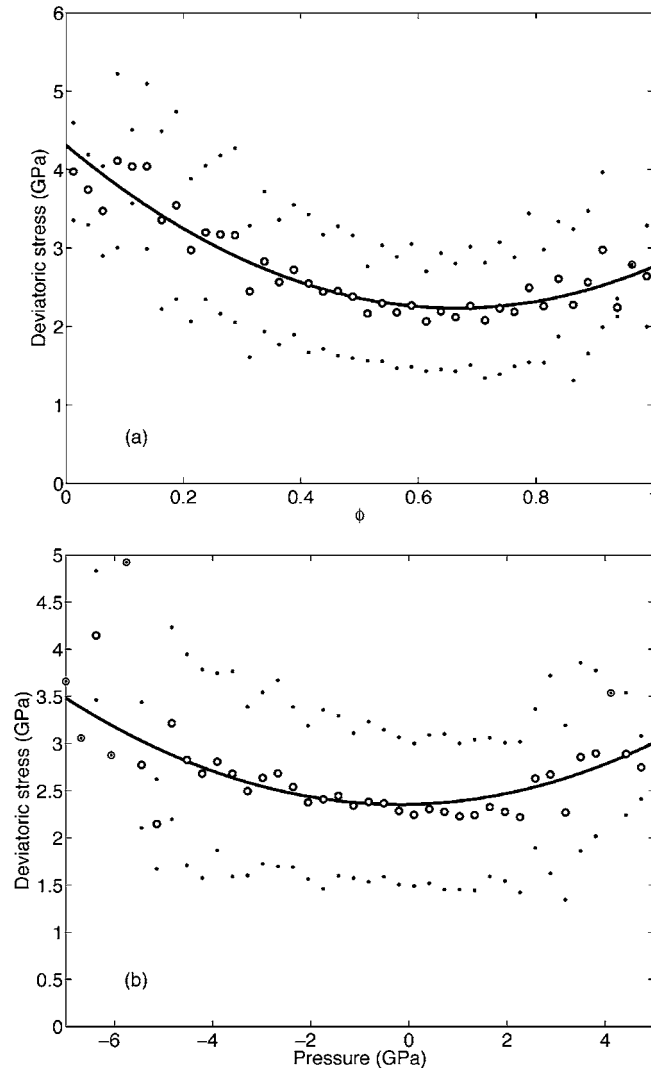


FIG. 13. Average dependence of the local deviatoric stress  $\bar{\sigma}(\tau)$  of triggering clusters on (a) the liquidlike mass fraction  $\phi$  of those clusters and (b) their pressure  $p(\tau)$ . Small dots denote the envelope of  $\pm 1$  standard deviation. Both of the dependencies exhibited are described well by a quadratic fit.

atomic distances present in each triggering cluster. To facilitate comparison to the bonding characteristics of bulk a-Si, this histogram was scaled in the same way as a radial distribution function (RDF) of bulk material is usually scaled.<sup>51</sup> Such a structure analysis process yields an “ensemble average RDF,” plotted in Fig. 14, for material comprising triggering clusters. Since the triggering clusters are compact, it is not surprising that they contain few atom pairs separated by distances larger than the second nearest-neighbor distance in bulk a-Si, as reflected by the vanishing of the ensemble-averaged RDF at large distances. Their compactness also explains the common occurrence of nearest-neighbor bonds. Within the second nearest-neighbor shell, however, the ensemble-averaged RDF reveals a striking deviation in the bonding environments of triggering clusters from those of bulk a-Si. Specifically, the split second nearest-neighbor peak of bulk a-Si is suppressed, while the bond length corresponding to the trough between its two parts is highly over-

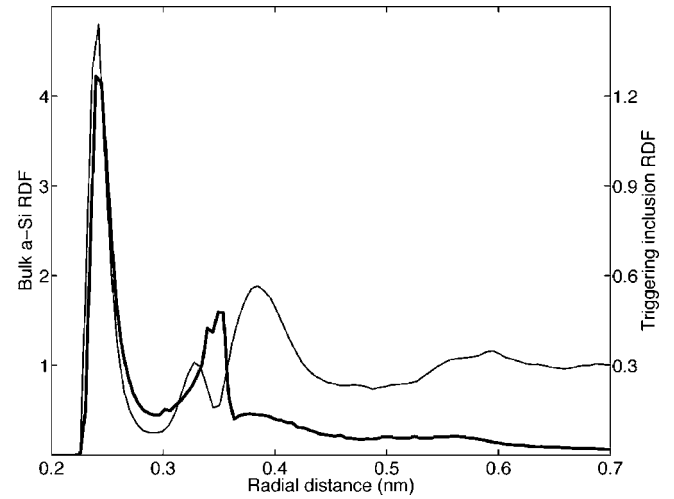


FIG. 14. A radial distribution function (RDF) compiled from interatomic distances among atoms comprising triggering clusters (thick line) is compared to a typical RDF for bulk a-Si in a state of steady flow (thin line). The two parts of the split second nearest-neighbor peak observed in bulk a-Si are missing from the triggering cluster RDF while bond lengths corresponding to the trough between them are overrepresented.

represented. This bond length is within the cutoff distance for direct atomic interaction in the SW potential [1.8 in reduced units, i.e., 0.377 nm (Ref. 11)].

In addition to the structural information contained in the atomic arrangement of each triggering cluster, characteristics of the kinematics of onset of stress relaxations can be found by investigating the shape of the normal mode whose stiffness vanishes (i.e., of the “soft mode” or CE). The relative atomic displacements contained in the CE at the onset of each stress relaxation can be used to find the relative changes in interatomic distances in each triggering cluster according to the formula

$$\dot{r}_{ij} = \frac{r_{ij,x}}{r_{ij}}(se_{j,x} - se_{i,x}) + \frac{r_{ij,y}}{r_{ij}}(se_{j,y} - s \cdot e_{i,y}) + \frac{r_{ij,z}}{r_{ij}}(se_{j,z} - se_{i,z}). \quad (16)$$

where  $e_{j,x}$  is the  $x$  component of the displacement of atom  $j$  from the complete unit CE vector  $\hat{e}$ ,  $r_{ij,x}$  is the  $x$  component of the position vector of atom  $j$  with respect to atom  $i$ , and  $\dot{r}_{ij}$  is the change of distance between the two atoms for displacements along the CE. Each CE is defined to within the arbitrary multiplicative constant  $s$ , as in Sec. VII [Eq. (14)]. For convenience, this constant is chosen in each case so that the greatest absolute value of change in interatomic distance in the triggering cluster is unity, i.e.,  $|\dot{r}_{ij}|_{\max} = 1$ . After all relative changes of interatomic distances in each of the 4201 triggering clusters have been computed, the average of their absolute values is found as a function of the interatomic distance itself. An analog of the ensemble-averaged RDF is thereby obtained except that, instead of characterizing the average *density* of triggering cluster material at a given interatomic separation, it specifies the average *absolute value*

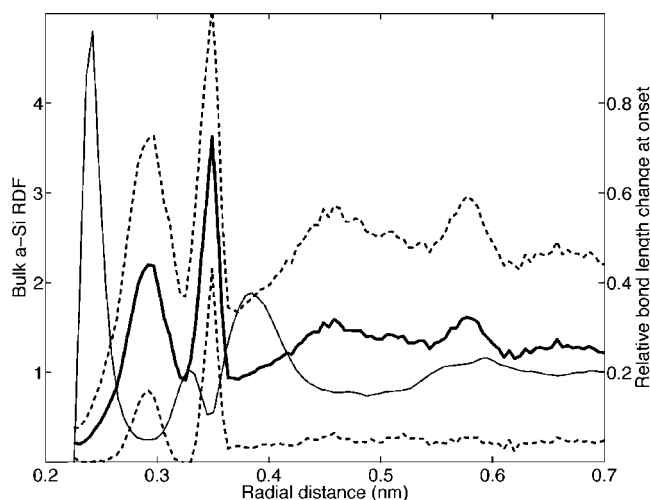


FIG. 15. The radial distribution of average relative bond-length changes in triggering clusters at onset of stress relaxations (thick solid line) is compared to a typical RDF for bulk a-Si in a state of steady flow (thin line). The thick dashed lines represent the envelope of  $\pm 1$  standard deviation. Bond lengths corresponding to the trough between two parts of the split second nearest-neighbor peak in a-Si undergo the largest relative length changes at onset of stress relaxations.

of the relative change in interatomic distance as a function of interatomic separation.

The function described above is presented in Fig. 15. It shows that the nearest-neighbor bond lengths in triggering clusters undergo the least relative length change at the onset of stress relaxations, i.e., they are the stiffest bonds. Meanwhile, the bond lengths corresponding to the trough of the split second nearest-neighbor peak in bulk a-Si undergo the most pronounced length changes at the onset of stress relaxations: they dominate the kinematics of triggering of internal structural transformations. To underscore their role in triggering local yielding, these bond lengths shall be given the suggestive name of instability-producing bonds (IPBs). There is a third bond length that undergoes relatively large length changes at the onset of stress relaxations. It is the length located between the first and second nearest-neighbor shells of bulk a-Si, as Fig. 15 shows. This bond, however, is not commonly present in the triggering clusters (Fig. 14) and thus is not accorded a role similar to that of the IPBs.

If IPBs are the fundamental structural components of the unit shearing events responsible for triggering plasticity in a-Si, then they must interact with their immediate atomic environments to produce shear strains. In particular, IPB length changes should induce rearrangements in the nearest-neighbor shells of the atoms at the IPB endpoints. These rearrangements must not involve significant displacements of nearest-neighbor atoms out of their shells since, according to Fig. 15, nearest-neighbor bond lengths do not change appreciably during the onset of stress relaxations. The rearrangements should therefore amount to the reshuffling of atoms within the nearest-neighbor shells themselves. For every nearest neighbor of atoms at IPB endpoints, such reshuffling can be described by changes in the two angles pictured in Fig. 16: one an axial rotation ( $\alpha$ ) and the other a lateral

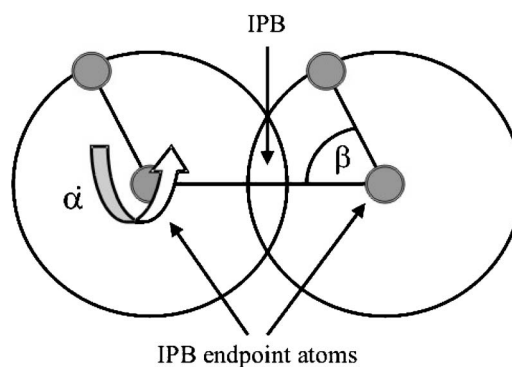


FIG. 16. Since nearest-neighbor bond lengths do not undergo significant length changes at onset of stress relaxations, the rearrangement of atoms in the nearest-neighbor shells of IPB endpoints can be described by changes in the axial angle  $\alpha$  and lateral angle  $\beta$ .

flexing ( $\beta$ ).

To characterize the nearest-neighbor distribution as a function of lateral flexing angle  $\beta$ , all such angles for all atoms in the 4201 triggering inclusions that are in the nearest-neighbor shells of IPB endpoint atoms were found. A histogram of these lateral flexing angles is presented in Fig. 17(a). Furthermore, the relative changes of lateral angles  $\beta$  at onset of stress relaxations can be determined directly from the shape of the CE, much as relative bond length changes can be found from the CE using Eq. (16). For ease of comparison to the relative length change of the underlying IPB,  $\beta$  for each atom was multiplied by its (relatively unchanging) distance to the IPB endpoint upon which it neighbors and then was divided by the relative length change of the underlying IPB (to avoid dividing by numbers close to zero, only IPBs with absolute values of relative length changes above 0.7 were considered). The quantities thus determined characterize lateral incremental atomic displacements tangent to their nearest-neighbor shells per unit length change of the underlying IPB. Plotting the averages of these relative tangential displacements against the lateral flexing angles at which they occur yields Fig. 17(b). Note the similarity in the analysis described above to the one carried out before on triggering cluster interatomic distances and their relative changes. Indeed, Fig. 17(b) is to Fig. 17(a) what Fig. 15 is to Fig. 14.

Figure 17(a) demonstrates that high concentrations of IPB endpoint nearest-neighbor atoms occur at lateral angles of about  $47^\circ$  and  $65^\circ$ . Of these two angles, the one at  $47^\circ$  exhibits the largest relative changes at onset of stress relaxations, as indicated in Fig. 17(b). Figure 17(b) also shows that changes in lateral angles are generally negatively correlated to the change in length of the underlying IPBs, i.e.,  $\beta$  increases when the underlying IPB length decreases and vice versa. It would be tempting to think that the nearest-neighbor atoms of IPB endpoints at lateral angles around  $47^\circ$  and  $65^\circ$  occur in some characteristic numbers or mutual configurations. No clear evidence, however, of such regularities was found. The results of the above analysis must be interpreted as characterizing the structure and kinematics of IPB endpoint nearest-neighbor shells *on average* with the under-

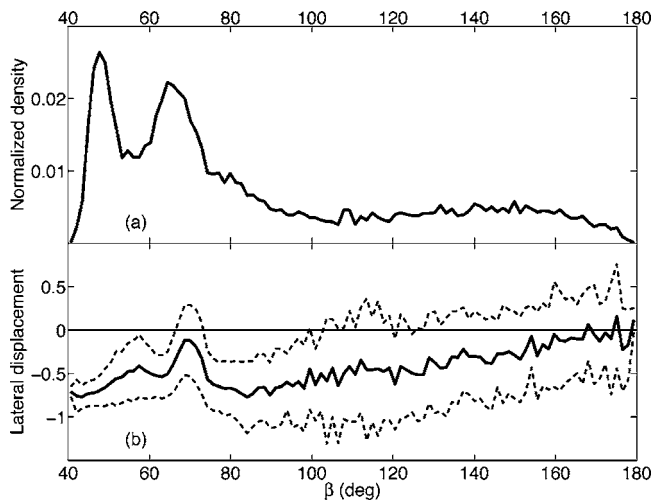


FIG. 17. The distribution of lateral bond angles  $\beta$  for IPBs triggering inclusions shows concentrations of atoms at  $47^\circ$  and  $65^\circ$  (a). The corresponding average lateral displacements (see Sec. VIII for definition) are negatively correlated to the length change of the underlying IPB and are greatest for atoms at lateral angles of about  $47^\circ$  (b). The dashed lines in (b) represent the envelope of  $\pm 1$  standard deviation.

standing that the environments of specific individual IPBs may vary. It is not inconceivable that if a more sophisticated “pattern recognition” scheme than the one described were applied, a finite catalog of typical atomic configurations surrounding IPB endpoints could be compiled. The compilation of such a catalog, however, was not attempted in this study.

A similar analysis to the one presented above was carried out for changes in the axial angles of rotation  $\alpha$ , but no readily recognizable characteristic kinematical behavior of the nearest neighbors of IPB endpoint atoms was found. Distributions of nearest-neighbor bond angles in the triggering clusters as well as of their relative changes were also investigated, but did not yield any unambiguous insights. Within the limits of the structure analysis schemes used in this study, therefore, it can be concluded that the IPBs and the associated regularities in the nearest-neighbor shells of their endpoint atoms are the only atomic arrangements characteristic of a-Si material comprising triggering clusters and leading to onset of local yielding. The number of IPBs per triggering cluster appears to be proportional to the number of atoms comprising the cluster, with an average of about 12 IPBs per cluster.

### IX. RECURRING ATOMIC BONDING CHANGES IN INELASTICALLY TRANSFORMING INCLUSIONS

To confirm that unit plastic events in a-Si consist of shear transformations involving IPBs and the nearest-neighbor shells of their endpoints, an analysis analogous to the one presented above was carried out on the transforming inclusions associated with the stress relaxations (Sec. V) that follow each triggering event. Although the kinematics of triggering clusters is described by the relative incremental atomic displacements in the CE, during the ensuing stress

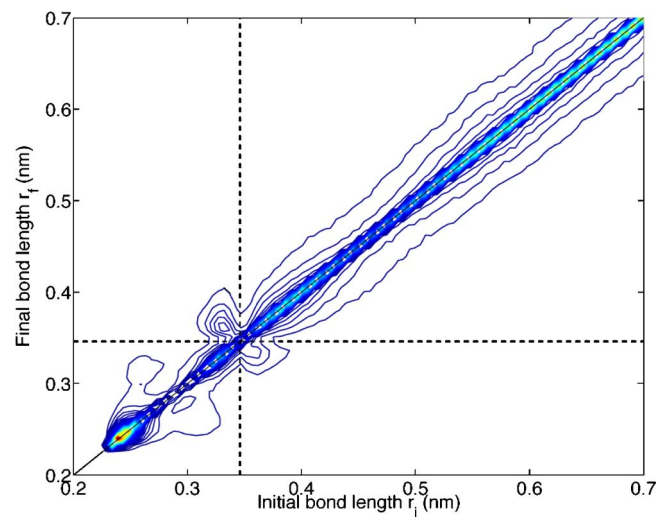


FIG. 18. (Color online) Plotting isocontours of distributions of initial vs final interatomic distances for atoms comprising transforming inclusions of material that deforms inelastically during stress relaxations reveals recurring bond-length changes. Most isocontours center on the diagonal, indicating bond lengths that do not change on average. The clearest departure from this trend occurs in the region shown by the intersecting dashed lines and indicates bond-length transitions across the IPB length ( $\sim 0.346$  nm).

relaxations each atom displaces by some finite amount with respect to all other atoms. Therefore, instead of evaluating the relative change in interatomic distances as before, the distance between each pair of atoms in each transforming inclusion at the onset was compared to the finitely different distance between the same pair after the stress relaxation had proceeded to completion. Thus, two interatomic distances are obtained for every pair of atoms in each inelastically transforming inclusion: one at the onset of the stress relaxation and one corresponding to the fully equilibrated final configuration. This calculation was performed in transforming inclusions for all 4201 stress relaxations observed in this study. All of the initial interatomic separations  $r_i$  collected in this way can be plotted against the corresponding final separations  $r_f$ , yielding a plot of points scattered in the plane. Points lying close to the diagonal in such a plot denote interatomic distances that do not change appreciably during a stress relaxation. Those lying below the diagonal correspond to distances that decrease, whereas those lying above the diagonal correspond to those that increase. For ease of visualization, a distribution density of these points can be compiled and isocontours of this distribution plotted.

Figure 18 shows the result of the analysis described above. Most interatomic distances do not undergo changes that commonly recur, as indicated by the fact that the isocontours are mostly centered on the diagonal. There is only one exceptional interatomic distance with nearby isolated off-diagonal isocontours: the distance corresponding to an IPB length ( $\sim 0.346$ -nm, Figs. 14 and 15). These isocontours indicate well-defined transitions of bond lengths from just below the IPB length to just above it, and vice versa. These transitions therefore correspond to bond-length migration between the two portions of the split second nearest-neighbor

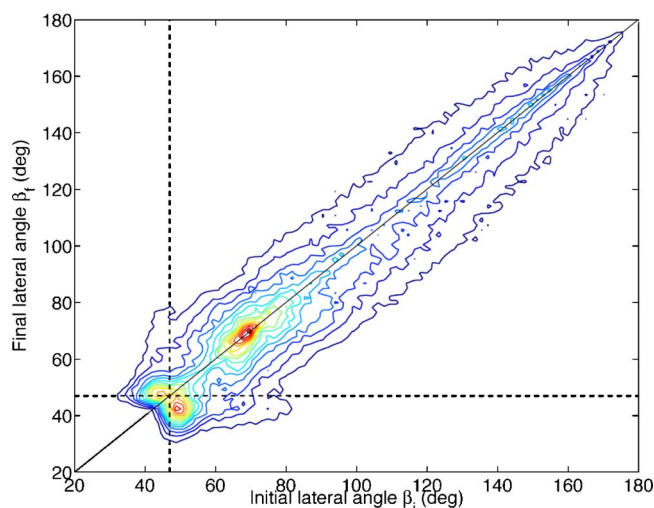


FIG. 19. (Color online) Plotting isocontours of distributions of initial vs final values of lateral angles  $\beta$  (Fig. 16) for atoms in the nearest-neighbor shells of endpoints of bonds that transition across the IPB length (Fig. 18) reveals recurring lateral-angle changes in the inelastically transforming inclusions. Most isocontours center on the diagonal, indicating angles that do not change on average. The clearest departure from this trend occurs in the region shown by the intersecting dashed lines and indicates lateral-angle transitions across the lateral angle of  $\sim 47^\circ$ .

peak in the RDF of bulk a-Si (Fig. 14) during discrete stress relaxations.

In addition to the behavior close to the IPB length, Fig. 18 indicates some activity in the nearest-neighbor shell. It is immediately clear, however, that this activity is mostly confined to the nearest-neighbor shell itself, i.e., that during a stress relaxation nearest-neighbor bonds are not commonly broken or formed in the inelastically transforming inclusion. This analysis does not imply that isolated bond breaking or reforming events do not take place, but rather that they are not characteristically recurring on average and therefore do not play a role of any prominence compared to that of transitions across the IPB length.

Changes in lateral angles of nearest neighbors of endpoint atoms (Fig. 16) of bond lengths that undergo a transition across the IPB length (Fig. 18) can be studied analogously to interatomic distance changes. For every atom in the nearest-neighbor shell of an endpoint of a bond length that crosses the IPB length, the initial and final values of the lateral angle  $\beta_i$  and  $\beta_f$  are computed. Isocontours of the distribution density of initial versus final lateral angle values are plotted in Fig. 19. It is evident that the only lateral angles that undergo transitions that recur on average are the same ones that exhibit the largest changes at the onset of stress relaxations [Fig. 17(b)], namely,  $\sim 47^\circ$ . Finally, Fig. 20 plots the increments in lateral angles against the increments in the underlying bond-length changes across the IPB length, showing that changes in lateral angles and the underlying bond lengths are negatively correlated, just as they are at onset of stress relaxations [Fig. 17(b)].

This analysis of recurring structure changes in transforming inclusions confirms that bond-length transitions in the second nearest-neighbor shell across the IPB length and the

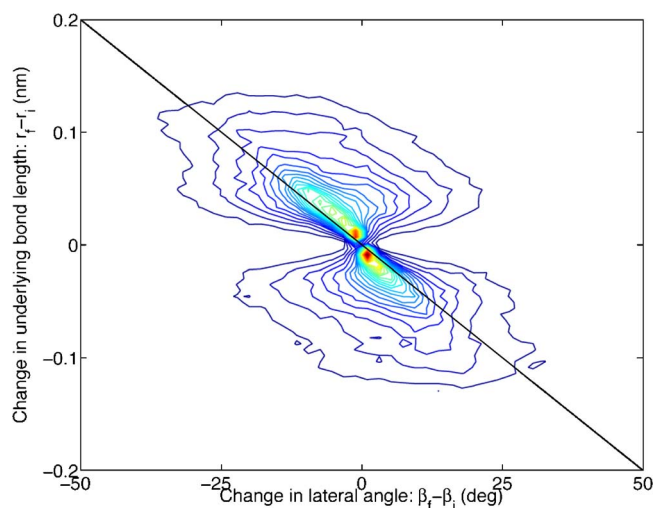


FIG. 20. (Color online) Plotting isocontours of distributions of lateral-angle changes ( $\beta_f - \beta_i$ ) against changes in length ( $r_f - r_i$ ) of the underlying bond (all of which undergo a transition across the IPB length, as indicated in Fig. 18) shows that the two are negatively correlated. This result agrees with the findings for kinematics of IPB environments in triggering inclusions at onset of stress relaxations [Fig. 17(b)].

associated distortions in their immediate atomic environments are the dominant features of the fundamental unit plastic events responsible for irreversible stress relaxations observed in this study. Figure 21 shows visualizations of two typical atomic configurations associated with these recurring unit events in the transforming inclusions. The number of such events in every stress relaxation was found to be linearly proportional to the size of the associated inelastically transforming inclusion with on average seven events for every ten inclusion atoms.

## X. DISCUSSION AND CONNECTION WITH EXPERIMENTAL FINDINGS

A study of the mechanisms of stress relaxation in a-Si was presented by Witvrouw and Spaepen in their investigation of viscoelasticity in a-Si.<sup>52</sup> Viscoelasticity and large-strain plasticity in a-Si may not at first glance appear to be related, but the results presented in the present study indicate the connection: regardless of the extent of inelastic stress relaxation, the underlying structure transformation is describable as an autocatalytic avalanche of unit events. Viscoelasticity therefore involves only small spatially isolated avalanches of such events triggered at low externally applied stresses. Meanwhile, fully developed plasticity involves large avalanches, triggered at the steady state flow stress, that repeatedly percolate through the entire system in close proximity to each other. The characteristics of the local yielding phenomenon that leads to the onset of relaxation, however, were found to be unrelated to the extent of the relaxation or the stress at which it was triggered. As was indicated in Sec. VIII, every triggering cluster contained on average 12 IPBs: bond lengths characteristic of the transition state of the structural components undergoing unit plastic transformations. Mean-

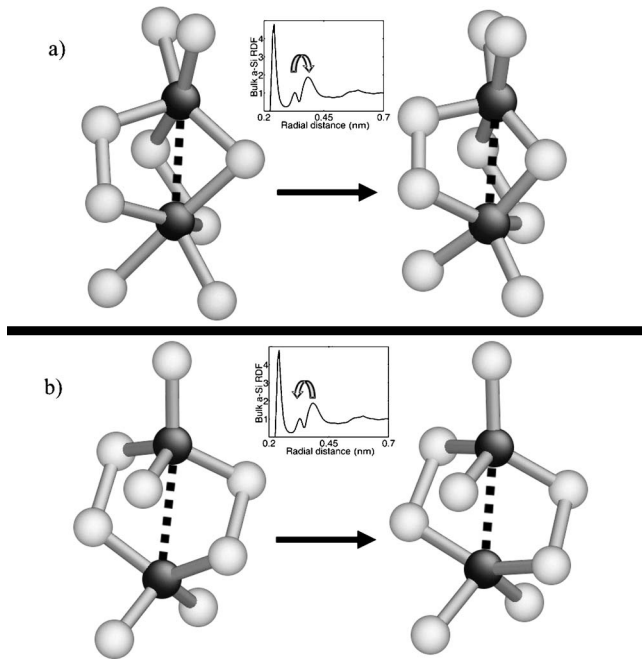


FIG. 21. Atomic configuration changes associated with nearest neighborhoods of bonds that undergo a transition across the IPB length are shown. Dark atoms correspond to endpoints of bonds that undergo this transition, whereas the light ones are their nearest neighbors. In (a), the bond undergoing the transition elongates beyond the IPB length, whereas in (b) it contracts below the IPB length. The atom that neighbors on both endpoints of the transitioning bond length in configuration (a) exhibits a lateral angle that crosses the threshold of  $47^\circ$  discussed in Fig. 19. There is no such atom in configuration (b), although lateral angles of the other nearest-neighbor atoms show a negative correlation to the underlying bond-length change, as demonstrated in Fig. 20.

while, Witvrouw and Spaepen concluded based on their study that activation of every viscoelastic relaxation requires the presence of more than one structural component, such as a bonding environment.

More information on the mechanisms of viscoelastic relaxation was obtained by Liu *et al.* in internal friction studies.<sup>53</sup> They found that the internal friction of a-Si could be reduced by hydrogenating the material by an atomic fraction of hydrogen of up to 1%, i.e., well in excess of the 0.07% hydrogen atomic fraction needed to passivate dangling bonds. Despite uncertainties concerning distribution of hydrogen in the sample,<sup>54</sup> this finding suggests that the atomic configurations responsible for local relaxations in a-Si may have enough common structural features to possess the chemical specificity to preferentially bond hydrogen. Unfortunately, no simulation studies have addressed the question of the effect of hydrogenation of a-Si on its susceptibility to undergo inelastic stress relaxations.

It is clear that neither of the experiments discussed above provides a definitive description of the geometry of the bonding environments responsible for inelastic relaxation in a-Si. Because, at present, individual atomic environments in amorphous materials cannot be directly imaged in the laboratory, however, no single experimental finding will likely suffice. Computer modeling will therefore continue to play a key role

in interpreting the experimental results, particularly by providing the basis for constructing models of homogenized behavior that take into account relevant details of the atomic configuration of amorphous materials as well as the dynamics of structural relaxations in them. Examples of such models—initially intended for metallic glasses—are the ones provided by Bulatov and Argon<sup>2</sup> as well as Falk *et al.*<sup>55</sup>

In the case of a-Si, analysis of the onset of stress relaxations and of the subsequent relaxation processes has shown that the transition state of a grouping of atoms undergoing a unit plastic event is geometrically characterized by the IPB length. Developing a complete theory of structure transitions for these groupings of atoms along the lines of that used to model the kinetics of plasticity in crystals,<sup>56</sup> however, requires a description of the properties of these groupings of atoms in their unloaded, stress-free state, both before and after a transition has taken place. Attempts at such a description, however, have not yielded satisfactory results so far. An alternate theoretical approach might focus on trying to understand the power-law distributions found in Secs. IV and VI in terms of possible connections to self-organized criticality.<sup>57</sup> Such an approach, however, was not pursued in this study.

Finally, although a-Si has special chemically specific features and is a pure substance, it shares many physical behaviors with other directionally bonded materials such as  $\text{SiO}_2$  and other unmodified inorganic glasses.<sup>58</sup> The mechanistic features of its plastic relaxations are therefore likely to be present in other directionally bonded pure materials. Indeed, the bond-length transitions across the IPB length described in this study bear a striking resemblance to the two-state mechanism of viscoelastic relaxation<sup>59</sup> proposed previously by Stranka for  $\text{SiO}_2$  based on ultrasonic attenuation measurements.<sup>60</sup>

## XI. CONCLUSION

The mechanisms of low-temperature plasticity in SW a-Si were investigated by external straining followed by relaxation using potential-energy minimization (PEM). Localized internal atomic rearrangements were found to accompany irreversible relaxations of the system stress. The number of atoms participating in these rearrangements was proportional to the deviatoric component of the corresponding increments of stress relaxation, suggesting that these rearrangements can be described as autocatalytic avalanches of unit shearing events. Investigation of a-Si at the mechanical thresholds for onset of stress relaxations demonstrated the existence of a local yielding criterion that must be satisfied for any given atomic cluster to start undergoing a structure transformation. Further analysis revealed that unit plastic shearing events in a-Si are characterized by the presence of instability-producing bonds (IPBs) whose length corresponds to the trough of the split second nearest-neighbor peak in the radial distribution function (RDF) for bulk SW a-Si. Inelastic relaxations consisting of many unit events involve transitions of bond length between these two portions of the split second nearest-neighbor peak.

## ACKNOWLEDGMENTS

We are grateful to D. M. Parks for his insight on the issue of distinguishing between elastically deforming matrix material and an inelastically transforming inclusion. The formalism presented in Sec. V was inspired by his comments. We are also indebted to S. Veprek, N. Marzari, S. Yip, A. de Vita, A. Needleman, R. Sharma, and M. Zimmermann for many useful discussions. This paper is based on work supported by

the NSF Graduate program and by the Defense University Research Initiative on NanoTechnology (DURINT) on “Damage- and Failure-Resistant Nanostructured and Interfacial Materials,” funded at the Massachusetts Institute of Technology by the Office of Naval Research under Grant No. N00014-01-1-0808. Salary assistance to M.J.D. was also provided by the Dean of the Graduate School and the Department of Mechanical Engineering at MIT.

\*Corresponding author. Email address: demkowitz@lanl.gov

- <sup>1</sup>M. J. Demkowitz and A. S. Argon, Phys. Rev. Lett. **93**, 025505 (2004).
- <sup>2</sup>M. J. Demkowitz and A. S. Argon, preceding paper, Phys. Rev. B **72**, 245205 (2005).
- <sup>3</sup>D. Deng, A. S. Argon, and S. Yip, Philos. Trans. R. Soc. London **329**, 549 (1989); **329**, 575 (1989); **329**, 595 (1989); **329**, 613 (1989).
- <sup>4</sup>V. V. Bulatov and A. S. Argon, Modell. Simul. Mater. Sci. Eng. **2**, 167 (1994); **2**, 185 (1994); **2**, 203 (1994).
- <sup>5</sup>D. J. Safarik, C. M. Cady, and R. B. Schwarz, Acta Mater. **53**, 2193 (2005).
- <sup>6</sup>A. S. Argon and L. T. Shi, in *Amorphous Materials: Modeling of Structure and Properties*, edited by V. Vitek, Metallurgical Society of AIME, Warrendale, PA, 279 (1983).
- <sup>7</sup>H. Eyring, J. Chem. Phys. **4**, 283 (1936).
- <sup>8</sup>A. S. Argon, in *Dislocation Modelling of Physical Systems*, ed. M. F. Ashby, R. Bullough, C. S. Hartley, and J. P. Hirth (Pergamon Press, Oxford, 1981) p. 393.
- <sup>9</sup>N. Bernstein, M. J. Aziz, and E. Kaxiras, Phys. Rev. B **61**, 6696 (2000).
- <sup>10</sup>F. Valiquette and N. Mousseau, Phys. Rev. B **68**, 125209 (2003).
- <sup>11</sup>F. H. Stillinger and T. A. Weber, Phys. Rev. B **31**, 5262 (1985).
- <sup>12</sup>J. Tersoff, Phys. Rev. Lett. **56**, 632 (1986).
- <sup>13</sup>H. Balamane, T. Halicioglu, and W. A. Tiller, Phys. Rev. B **46**, 2250 (1992).
- <sup>14</sup>M. Z. Bazant, E. Kaxiras, and J. F. Justo, Phys. Rev. B **56**, 8542 (1997).
- <sup>15</sup>W. D. Luedtke and U. Landman, Phys. Rev. B **40**, 1164 (1989).
- <sup>16</sup>M. D. Kluge and J. R. Ray, Phys. Rev. B **37**, 4132 (1988).
- <sup>17</sup>P. Keblinski, S. R. Phillpot, D. Wolf, and H. Gleiter, Phys. Rev. Lett. **77**, 2965 (1996).
- <sup>18</sup>P. Keblinski, S. R. Phillpot, D. Wolf, and H. Gleiter, Acta Mater. **45**, 987 (1997).
- <sup>19</sup>S. Sastry and C. A. Angell, Nat. Mater. **2**, 739 (2003).
- <sup>20</sup>F. A. McClintock and A. S. Argon, *Mechanical Behavior of Materials* (Addison-Wesley, Reading, MA, 1966).
- <sup>21</sup>A. R. Leach, *Molecular Modelling: Principles and Applications* (Prentice Hall, Harlow, England, 2001).
- <sup>22</sup>E. Polak and G. Ribiere, Rev. Fr. Inform. Rech. Oper. **16**, 35 (1969).
- <sup>23</sup>D. P. Bertsekas, *Nonlinear Programming* (Athena Scientific, Belmont, MA, 1999).
- <sup>24</sup>R. P. Brent, *Algorithms for Minimization without Derivatives* (Prentice-Hall, Englewood Cliffs, NJ, 1973).
- <sup>25</sup>Netlib, <http://www.netlib.org/>

- <sup>26</sup>I. S. Duff, A. M. Erisman, and J. K. Reid, *Direct Methods for Sparse Matrices* (Oxford University Press, London, 1986).
- <sup>27</sup>C. C. Paige and M. A. Saunders, SIAM (Soc. Ind. Appl. Math.) J. Numer. Anal. **12**, 617 (1975).
- <sup>28</sup>R. B. Lehoucq, D. C. Sorensen, and C. Yang, *ARPACK Users' Guide: Solution of Large-Scale Eigenvalue Problems with Implicitly Restarted Arnoldi Methods* (SIAM, Philadelphia, 1998).
- <sup>29</sup>K. Maeda and S. Takeuchi, Philos. Mag. A **44**, 643 (1981).
- <sup>30</sup>A. Kabla and G. Debregeas, Phys. Rev. Lett. **90**, 258303 (2003).
- <sup>31</sup>N. S. O. Ekunwe and J. D. Lacks, Phys. Rev. B **66**, 212101 (2002).
- <sup>32</sup>P. H. Mott, A. S. Argon, and U. W. Suter, Philos. Mag. A **67**, 931 (1993).
- <sup>33</sup>A. S. Argon, in *Physical Metallurgy*, edited by R. W. Cahn and P. Haasen (North-Holland, Amsterdam, 1996) p. 1957.
- <sup>34</sup>D. J. Lacks, Phys. Rev. E **66**, 051202 (2002).
- <sup>35</sup>A. C. Lund and C. A. Schuh, Mater. Res. Soc. Symp. Proc. **806**, MM7.4.1 (2004).
- <sup>36</sup>C. Maloney and A. Lemaitre, Phys. Rev. Lett. **93**, 016001 (2004).
- <sup>37</sup>J. D. Eshelby, Proc. R. Soc. London, Ser. A **241**, 376 (1957).
- <sup>38</sup>A. S. Argon and H. Y. Kuo, Mater. Sci. Eng. **39**, 101 (1979).
- <sup>39</sup>D. L. Malandro and D. J. Lacks, J. Chem. Phys. **110**, 4593 (1998).
- <sup>40</sup>P. H. Mott, A. S. Argon, and U. W. Suter, J. Comput. Phys. **101**, 140 (1992).
- <sup>41</sup>M. L. Falk and J. S. Langer, Phys. Rev. E **57**, 7192 (1998).
- <sup>42</sup>M. F. Horstemeyer and M. I. Baskes, Mater. Res. Soc. Symp. Proc. **578**, 15 (2000).
- <sup>43</sup>R. C. Singleton, Commun. ACM **12**, 185 (1969).
- <sup>44</sup>D. L. Malandro and D. J. Lacks, J. Chem. Phys. **107**, 5804 (1997).
- <sup>45</sup>J. Guckenheimer and P. Holmes, *Nonlinear Oscillations, Dynamical Systems, and Bifurcations of Vector Fields* (Springer-Verlag, Berlin, 1983).
- <sup>46</sup>J. D. Crawford, Rev. Mod. Phys. **63**, 991 (1991).
- <sup>47</sup>R. Blinc and B. Zeks, *Soft Modes in Ferroelectrics and Antiferroelectrics* (North-Holland, Amsterdam, 1974).
- <sup>48</sup>R. S. Elliot, J. A. Shaw, and N. Triantafyllidis, J. Mech. Phys. Solids **50**, 2463 (2002).
- <sup>49</sup>J. M. T. Thompson and G. W. Hunt, *A General Theory of Elastic Stability* (Wiley, London, 1973).
- <sup>50</sup>J. M. T. Thompson and P. A. Shorrock, J. Mech. Phys. Solids **23**, 21 (1975).
- <sup>51</sup>M. P. Allen and D. J. Tildesley, *Computer Simulation of Liquids* (Oxford University Press, London, 2000).
- <sup>52</sup>A. Witvrouw and F. Spaepen, J. Appl. Phys. **74**, 7154 (1993).

- <sup>53</sup>X. Liu, B. E. White, Jr., R. O. Pohl, E. Iwanizcko, K. M. Jones, A. H. Mahan, B. N. Nelson, R. S. Crandall, and S. Veprek, *Phys. Rev. Lett.* **78**, 4418 (1997).
- <sup>54</sup>X. Liu, P. O. Pohl, and R. S. Crandall, *Mater. Res. Soc. Symp. Proc.* **557**, 323 (1999).
- <sup>55</sup>M. L. Falk, J. S. Langer, and L. Pechenik, *Phys. Rev. E* **70**, 011507 (2004).
- <sup>56</sup>U. F. Kocks, A. S. Argon, and M. F. Ashby, *Thermodynamics and Kinetics of Slip* in *Progress in Materials Science*, edited by B. Chalmers, J. W. Christian, and T. B. Massalski (Pergamon Press, New York, 1975), Vol. 19.
- <sup>57</sup>H. J. Jensen, *Self-Organized Criticality: Emergent Complex Behavior in Physical and Biological Systems* (Cambridge University Press, Cambridge, England, 1998).
- <sup>58</sup>C. A. Angell, S. Borick, and M. Grabow, *J. Non-Cryst. Solids* **205–207**, 463 (1996).
- <sup>59</sup>J. Jackle and L. Piche, *J. Non-Cryst. Solids* **20**, 365 (1976).
- <sup>60</sup>R. E. Stranka, *Phys. Rev.* **123**, 2020 (1961).